ACS OMEGA

Open Access

http://pubs.acs.org/journal/acsodf

Article

Manganese Doping in Biomass Derived Carbon Dots Amplifies White Light-Induced Antibacterial Activity

Mohammad Tariq, Saurabh Shivalkar, Hammad Hasan, Amaresh Kumar Sahoo,* and Md Palashuddin Sk*

Cite This: *ACS Omega* 2023, 8, 49460−49466

Read Online

ACCESS | Metrics & More | Article Recommendations | Supporting Information

ABSTRACT: The prevalence of antibiotic-resistant bacterial infections demands effective alternative therapeutics of antibiotics, whereas biocompatible zero-dimensional nanomaterials are an excellent option due to their small size. In this study, we report the one-step hydrothermal approach that was used to synthesize luminescent manganese doped carbon dots (Mn-Cdots) with an efficient quantum yield of 9.2% by employing green *Psidium guajava L.* (Guava) leaf as the precursor. High-resolution microscopy TEM was used to investigate the average particle size of Mn-Cdots, which was found to be 2.9 ± 0.045 nm. The structural properties and elemental composition of Mn-Cdots were analyzed by FTIR, XRD, EPR, and XPS spectroscopy, and the optical properties of Mn-Cdots were examined by UV−visible and fluorescent spectroscopy. Light-mediated antibacterial activity of Mn-Cdots was investigated by Gram-negative bacteria *E. coli* under white, blue, and yellow light. The doping effect of a minute quantity of Mn in Mn-Cdots increased the level of ROS generation in the presence of white lights compared to Cdots. Thus, Mn-Cdots might act as potent antibacterial agents.

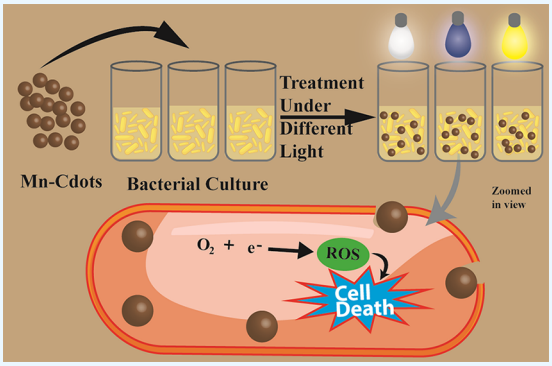

INTRODUCTION

The emergence of antibiotics for the remediation of potentially lethal infections is one of modern medicine's greatest achievements. However, this has led to the development of resistance to their antimicrobial effect. Moreover, multidrug resistance (MDR) and extensive drug-resistant (XDR) bacterial infection cause a huge number of fatalities annually.[1] Furthermore, the number of approved antibiotics in the past decade has been gradually decreasing due to a longer process of optimization, low economic incentives, and several regulatory requirements.[2] It has created an urgent call for the development of alternative approaches for the treatment of microbial infection as well as the development of novel antimicrobial agents.[3] Today, there are numerous methods being used for the synthesis of antimicrobial agents from natural products, the alteration of existing antibiotics, and the combination of two or more antibiotics.[4] Nanomaterials like metal nanoparticles (Ag, Au, Cu NPs), metal oxide nanoparticles (ZnO, CuO, AgO, Fe_2O_3 NPs), and inorganic nonmetallic nanoparticles (carbon-based nanomaterials, black phosphorus, Si QDs) have been found to be promising antibacterial agents.[5] They have a large surface area, which provides superior multivalent interaction capacity with microorganisms and the ability to infiltrate into the cell wall of bacteria and disrupt the functioning of bacterial cells, which influences bacterial growth. However, carbon-based nanomaterials have attracted much attention due to their biocompatibility and low toxicity compared to metal/semiconducting nanomaterials.

In this context, carbon dots (Cdots), which are often classified as small carbon nanoparticles with diameters up to 10 nm, are commonly known for their excellent optical properties and utilized in biological applications such as drug delivery, biotherapy, bioimaging, biosensing, and gene transmission and as antimicrobial agents.[6] Cdots have found their place in biology-related applications because of low toxicity and biocompatibility. Recently, Cdots have become popular as nanoantibacterial agents and are considered a potential candidate to replace antibiotics.[7,8] Several reports suggested that Cdots exhibit antimicrobial properties without photoexcitation. Multiple factors like precursors, size, amphiphilicity, surface charge, and functionality can tune the antimicrobial properties of Cdots.[7,8] Along with their physiochemical properties, fascinating optical properties of Cdots are employed for antimicrobial applications. Cdots under photoexcitation-photodynamics exhibit excellent antimicrobial properties. Among other antibacterial strategies for Cdots, the light-

Received: October 30, 2023
Revised: November 21, 2023
Accepted: November 23, 2023
Published: December 14, 2023

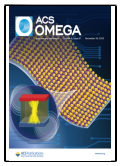

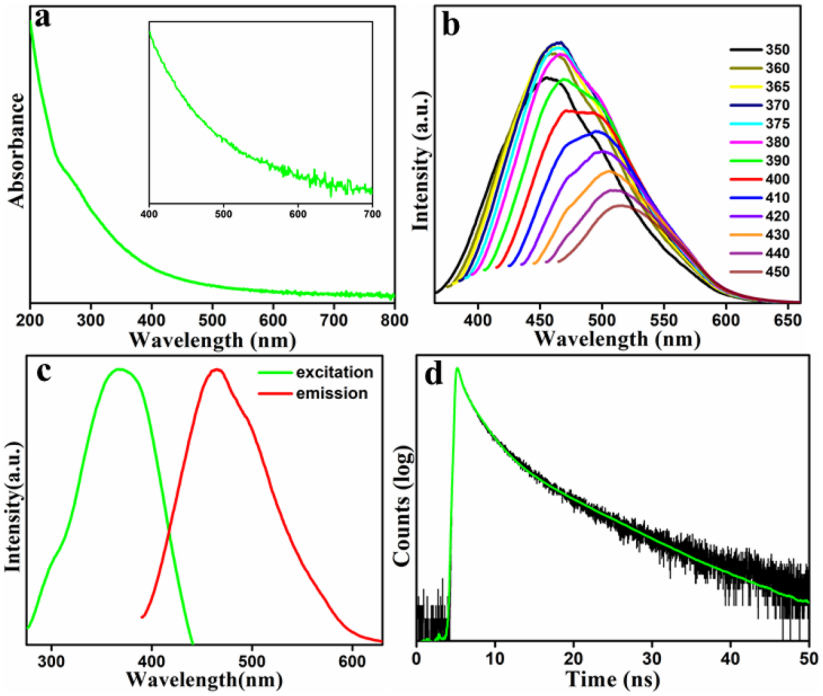

Figure 1. (a) UV−visible absorption spectrum of Mn-Cdots (0.25 mg/mL) dispersed in water (inset figure represents expanded UV−visible spectrum of Mn-Cdots in the range of 400−700 nm). (b) Emission characteristics of Mn-Cdots (0.5 mg/mL) dispersed in water, excited in the wavelength range of 350 to 450 nm. (c) Excitation spectrum of Mn-Cdots (peak centered at 370 nm), corresponding to the emission peak at 464 nm. (d) TRPL decay profile of Mn-Cdots.

induced photoexcitation-photodynamics strategy is an effective and efficient mechanism to combat bacterial resistance.

Apart from the hetero doping atom (like N, P, S, etc.), metal-doped Cdots are gaining interest in controlling the physicochemical properties of Cdots.[9−11] Metal ion doping in Cdots has been introduced to tune their electronic structure and chemical composition. Metal doping can regulate the electron density and energy gap in Cdots, which are essential for tuning the physical and chemical properties of Cdots. Manganese (Mn) is an essential element in the human body, playing a significant role in the development of cofactors for many enzymes.[12] Mn-based complexes are not very toxic; therefore, few reports are available of Mn-doped Cdots for magnetic resonance imaging applications.[13−15] Also, Mn-doped Cdots are found to be promising for biological applications.[16−19] However, photoactivated Mn-doped Cdots have not yet been extensively reported as antibacterial agents. Herein, we develop Mn-doped Cdots (Mn-Cdots) using *Psidium guajava L.* leaves (guava leaves) as a carbon source *via* a one-step hydrothermal method. Then, we employ photoexcited Mn-Cdots with 2,2′-azino-bis [3-ethylbenzothiazoline-6-sulfonic acid] (ABTS) under blue, yellow, and white light. White light-induced photoexcited Mn-doped Cdots with ABTS exhibit excellent antibacterial activity. The minimum inhibitory concentration (MIC) is determined to be 1.16 mg/mL. The inhibition of bacterial growth occurs due to the generation of reactive oxygen species (ROS). Moreover, the ABTS in the presence of photoexcited Mn-Cdots converts into its oxidant ($ABTS^{\bullet+}$) that further enhances the generation of radical species of Mn-Cdots under white light and, therefore, promotes the generation of ROS, which inhibits bacterial growth more effectively during the antibacterial mechanism.

EXPERIMENTAL SECTION

Synthesis of Mn-Doped Cdots. Fresh leaves of *Psidium guajava L.* (guava leaves) were collected from the guava plants on the AMU campus and washed with water. Then, 15 g of dried leaves was ground using a mortar pestle. After the grinding, the powder form of leaves was boiled in deionized water at 90 °C for 5 h. The supernatant, which includes extracted products of the reaction mixture, was collected in a 250 mL beaker with the help of Whatman filter paper. The extracted aqueous solution was concentrated up to 5 mL using an oven at 70 °C. Further, 0.2 mmol of manganese sulfate monohydrate was added to the concentrated solution (*i.e.*, 5 mL), and the carbonization reaction was performed at 180 °C for 5 h in a muffle furnace. The synthesized hydrothermal product was purified by using dialysis techniques. The dialysis was performed using 1 kDa (benzoylated dialysis bag) for 24 h.

Characterization of Mn-Cdots. The optical properties of Mn-Cdots were studied with the help of a PerkinElmer LAMBDA-45 spectrophotometer and HITACHI-F2500 fluorometer. FTIR analysis was performed by PerkinElmer infrared spectrometer. SEM images of the sample were recorded by using a JEOL JSM 6510LV electronic microscope. An XPS study was carried out with the help of an ESCA Multilab 2000. EPR and powder XRD of Mn-Cdots were measured using a JEOL JES FA200 instrument and Rigaku Smart lab X-ray diffractometer operating with a Cu Kα source (λ = 1.54 Å), respectively.

Antibacterial Activity Study. An antibacterial activity study was performed using ampicillin-resistant green fluorescence protein (GFP)-expressing recombinant *E. coli* as a model bacterial species. For this purpose, different sets of experiments were performed using *E. coli* under different light conditions. Three sets of 4 × 3 mL of freshly prepared LB

https://doi.org/10.1021/acsomega.3c08586
ACS Omega 2023, 8, 49460−49466

broth were taken in the test tubes. The three sets represent different light conditions (white, blue, and yellow). To evaluate the photosensitive properties, the Mn-Cdots were subjected to different colors of light, i.e., cool white (peak centered at λ = 460 nm), blue (λ = 425 nm), and yellow (λ = 590 nm) light and dark conditions in the presence of ABTS and inoculated *E. coli*. These lights were given by using two smart LED bulbs (Smitch SB010-B22) of 10 W each from the top. A control experiment was also performed with only ABTS in each set. For further confirmation, a positive control experiment was also carried out in the presence of only Cdots. After 12 h, bacterial growth was observed by measuring the absorbance (at 595 nm), representing the optical density (OD).

RESULTS AND DISCUSSION

The biomass-derived Mn-doped Cdots were synthesized from abundantly available guava leaves using a hydrothermal method. Guava leaves contain several medicinally important phytochemicals (such as tannic and flavonoid derivatives) and excellent carbon sources.[20] After purification, Mn-Cdots were redispersed in deionized water for further characterization. Figure 1a demonstrates the absorption characteristics of Mn-Cdots, which displays an absorption peak at 276 nm with a plateau-type absorption tail. The absorption peak at 276 nm is assigned to the $\pi-\pi^*$ transition graphitic core of Mn-Cdots.[21] The plateau-type absorption tail is observed, possibly due to the n$-\pi^*$ surface states of Mn-Cdots.[21] Then, the photophysical behavior of the aqueous solution of the Mn-doped Cdots was characterized. Figure 1b demonstrates the excitation tunable photoluminescence of Mn-Cdots, which were recorded in the excitation range 350 to 450 nm. The emission behavior of Mn-Cdots indicates the maximum emission intensity at 464 nm when excite at 370 nm (Figure 1c). Also, shifting of the emission maximum peak is observed with increasing excitation wavelength. The quantum yield of Mn-Cdots was found to be 9.2% with reference to quinine sulfate in 0.1 M H_2SO_4. Further, the time-resolved photoluminescence (TRPL) spectrum of Mn-Cdots confirmed the triexponential decay profile with an average lifetime (τ_{av}) of 3.36 ns (Figure 1d). The TRPL measurement was performed using a 375 nm excitation laser source.

The formation and morphology of Mn-Cdots were revealed in a transmission electron microscopy (TEM) study (Figure 2). TEM images confirmed the average size of 2.9 ± 0.045 nm. Further, high-resolution TEM (HRTEM) analysis indicates the *d*-spacing value of 0.21 nm, which corresponds to the lattice plane (001) of graphite carbon (Figure 2b).[13] We performed XPS experiments to gain insight into the elemental compositions and chemical nature of elements in Mn-Cdots. The XPS measurement result is presented in Figure 3. As shown in Figure 3, Mn-Cdots contain C, O, S, N, Mn, and Mg. Notably, guava leaf extraction naturally contains Mg, and therefore, the composition of Mn-Cdots indicates the presence of Mg.[22] Further, deconvoluted high-resolution spectra of C_{1s}, O_{1s}, S_{2p}, Mn_{2p}, and Mg_{2p} are demonstrated in Figure 3b−f. Analysis of the deconvoluted C_{1s} spectrum suggests the presence of C−C/C=C (284.4 eV), C−O/C−N (286.8 eV), C−NH_2 (293.1 eV), and a satellite peak due to π to π^* transition (296.2 eV)[23] in Mn-Cdots (Figure 3b). The deconvoluted signal of the O_{1s} spectrum indicates the presence of C−O/C=O (531.7 eV) functionalities, and the S_{2p} spectrum implies S−C (162.7 eV) and S=O (168.5 eV) in Mn-Cdots (Figure 3c,d). The high-resolution spectrum of Mn_{2p} confirms the appearance of typical $Mn_{2p3/2}$ (641.3 eV) and $Mn_{2p1/2}$ (653.7 eV) peaks, indicating the Mn^{2+} oxidation state of manganese in Mn-Cdots (Figure 3e).[14] The deconvoluted high-resolution Mg_{2p} band in Figure 3f shows the peaks at 48.1 eV (Mg−C) and 49.4 eV (Mg−O).[22] Energy dispersive X-ray (EDX) analysis and elemental mapping further demonstrates the presence of (weight %) 35.01% C, 60.78% O, 1.57% S, 0.81% Mn, and 1.82% Mg (Table S1 and Figure S1). The nitrogen element was not detected by EDX; however, it was detected during recording of the XPS spectrum. This is due to the presence of a trivial quantity of nitrogen in Mn-Cdots. Further, EPR measurement results also endorse manganese doping in divalent form (Figure S2).[24,25] Then, we carried out powder XRD measurement to characterize the composition or crystalline structure (Figure S3). In Figure S3, the XRD pattern confirms the presence of divalent Mn in Mn-Cdots (JPCD: 40-1289).[26] The XRD analysis result further resembles the results of XPS and EPR measurements, *i.e.*, the divalent oxidation state of manganese. Additionally, the surface functionalities of Mn-Cdots were characterized with the help of FTIR analysis. The FTIR spectrum (Figure S4) indicates the presence of −OH, C−H, C=C/C=N, C−O/C−N, =C−H, and Mn−O functional groups in Mn-Cdots, and their respective frequencies are $\nu_{(-OH)}$ 3374 cm^{-1}, $\nu_{(-C-H)}$ 2924 cm^{-1}, $\nu_{(C=C/C=N)}$ 1624 cm^{-1}, $\delta_{(C-H)}$ 1426 cm^{-1}, $\nu_{(C-O/C-N)}$ 1089 cm^{-1}, $\delta_{(=C-H)}$ 724 cm^{-1}, and $\nu_{(Mn-O)}$ 615 cm^{-1}.

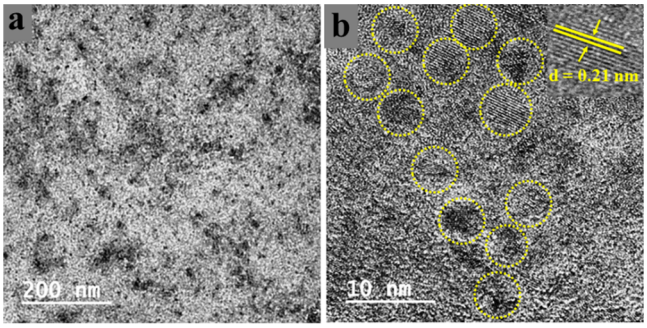

Figure 2. (a) TEM images of Mn-Cdots (scale bar at 200 nm). (b) High-resolution TEM (HRTEM) image indicating the formation of Mn-Cdots with average sizes of 2.9 ± 0.045 nm (scale bar at 10 nm).

Further, guava-leaf-derived Cdots were synthesized using a hydrothermal method as a control for antibacterial study. The synthesis protocol is given in the Supporting Information (SI). The detailed characterization of Cdots was performed using various techniques such as TEM, absorption spectroscopy, fluorescence spectroscopy, EPR, FTIR, XPS, EDX, etc. and are demonstrated in Figures S5−S8. Cdots contain (weight %) 40.83% C, 52.37% O, 3.07% S, and 3.74% Mg (Table S2 and Figure S8). Like Mn-Cdots, the nitrogen element was not detected during the EDX measurement, but the XPS study revealed the presence of a trivial quantity of nitrogen in Cdots. Notably, elemental analysis and the XPS study confirm that the Cdots contain Mg_{2p} inherently. The source of Mg_{2p} is the precursor guava leaves. Also, the absence of a manganese XPS signal in Cdots refers to the successful doping of manganese in Mn-Cdots.

Further, the stability of Mn-Cdots under different conditions, such as pH, ionic strengths, and UV light exposure, was studied by monitoring the photoluminescence of Mn-

https://doi.org/10.1021/acsomega.3c08586
ACS Omega 2023, 8, 49460−49466

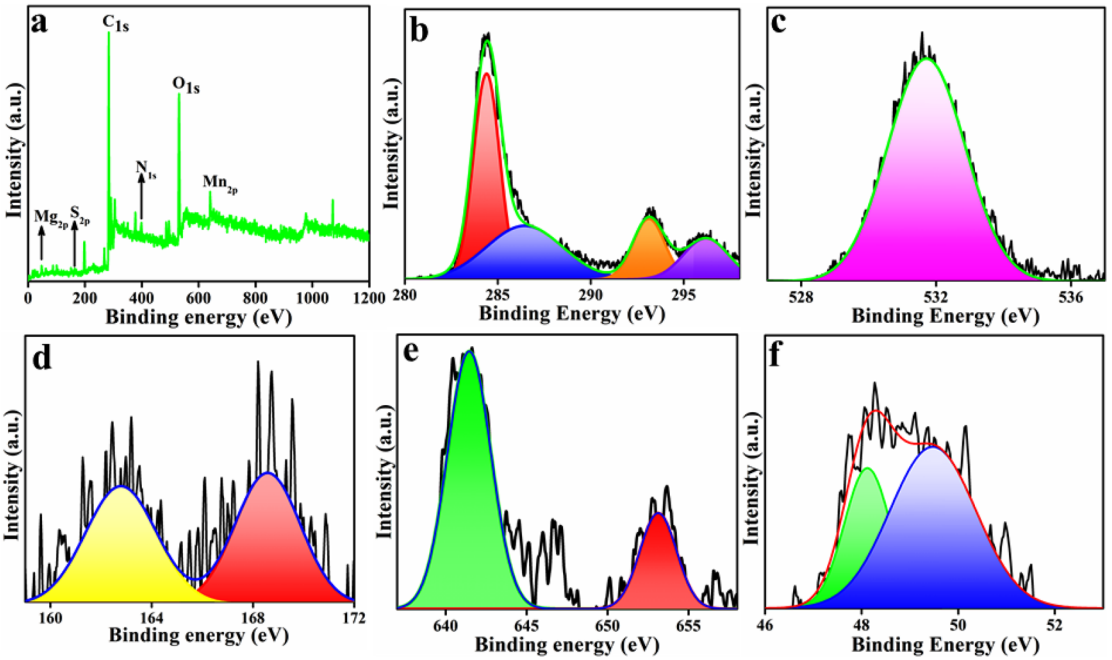

Figure 3. (a) Full scan XPS spectrum of Mn-Cdots, deconvoluted high-resolution C_{1s} signal (b), O_{1s} signal (c), S_{2p} signal (d), Mn_{2p} signal (e), and Mg_{2p} signal (f).

Cdots at an excitation of 370 nm and emission of 464 nm. Figure S9 indicates that the emission of Mn-Cdots is stable under different high salt concentrations. The pH dependence study demonstrates the almost constant emission behavior of Mn-Cdots (Figure S10). However, a slight increase in fluorescence of Mn-Cdots at pH = 7 was observed. The time-dependent photostability experiment also shows the stability of Mn-Cdots under exposure to 365 nm UV light (Figure S11).

Antibacterial Activity of Mn-Cdots. Further, we explored the antibacterial activity of Mn-Cdots. For this purpose, an ampicillin-resistant green fluorescence protein (GFP)-expressing recombinant *E. coli* was used to model bacterial species. Later, a time-dependent study was conducted to examine the effect of Mn-Cdots on the bacterial strain. First, we tried to establish the photosensitive nature of the Mn-Cdots for their antibacterial activity. To evaluate the photosensitive properties, the Mn-Cdots were subjected to different colors of 20 W light, *i.e.*, white, blue, and yellow light, in the presence of ABTS and inoculated *E. coli*. A control experiment was also conducted with only ABTS and dark conditions to establish the hypothesis. After 12 h, bacterial growth was observed by measuring the absorbance/optical density (OD) at 595 nm. Furthermore, inhibition of bacterial growth was observed, confirming the antibacterial nature of Mn-Cdots under each light condition. However, more than 50% growth inhibition was observed when the cells were placed under an incubator in the presence of white light. The MIC of Mn-Cdots was measured to be 0.33 mg/mL (D1), 0.83 mg/mL (D2), and 1.16 mg/mL (D3) with 0.42 mg/mL of ABTS (Figure 4). Furthermore, under similar MIC concentrations, no significant antibacterial activity was observed under dark conditions. Moreover, negligible antibacterial activity was observed with 0.42 mg/mL ABTS only. White light is generated from the mixing of red, green, and blue light. The expanded view of the UV−visible spectrum of Mn-Cdots shows that the Mn-Cdots can strongly absorb

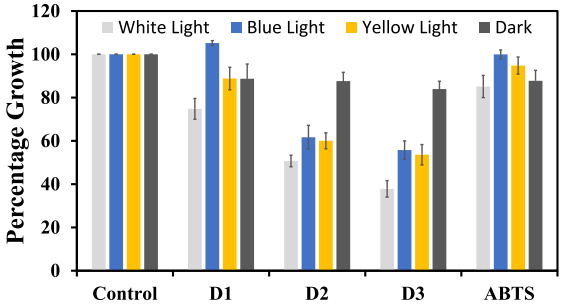

Figure 4. Normalized dose-dependent antibacterial activity measurement on *E. coli* using Mn-Cdots with ABTS under white, blue, and yellow light.

visible light in the whole range of 400−700 nm (Figure 1a).[27] Therefore, the superior antibacterial activity of Mn-Cdots was noted under white light compared to that under yellow and blue light.

However, after optimizing the concentration of ABTS and Mn-Cdots, it was observed that the antibacterial activity was increased by up to 90% when the setup was placed under the standard bacteria growth condition (incubation) in the presence of white light (Figure 5). The results demonstrated that 40% lesser ABTS concentration in the previous doses on Mn-Cdots provides better antibacterial activity. More than 85% growth inhibition was observed in the same MIC doses but with 0.25 mg/mL of ABTS. Moreover, negligible antibacterial activity was observed with 0.25 mg/mL of ABTS. Although, under similar conditions and doses of Cdots, no significant antibacterial effect was observed.

Figure 6 illustrates the results of the SEM investigation to compare the morphology of *E. coli* before and after treatment with 1.16 mg/mL of Mn-Cdots. Compared to untreated *E. coli* (Figure 6a), the SEM image of treated *E. coli* with Mn-Cdots (Figure 6b) shows damage to the bacterial cell walls. It is,

https://doi.org/10.1021/acsomega.3c08586
ACS Omega 2023, 8, 49460−49466

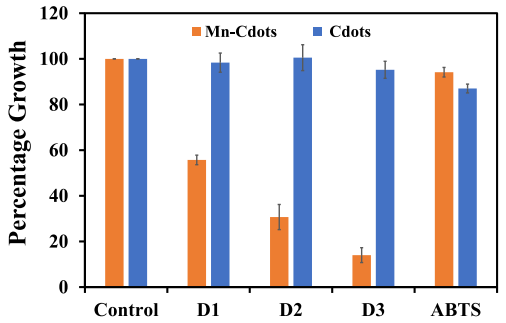

Figure 5. Dose-dependent antibacterial activity measurement on *E. coli* using Mn-Cdots with ABTS under standard bacteria growth conditions under white light.

conversely, clear that Mn-Cdots produce ROS that can disrupt the membrane of bacteria.

Oxidative Stress Measurement *via* the NBT Test. It was found that reactive oxygen species (ROS) generation may be responsible for bacterial growth inhibition. Therefore, a nitroblue tetrazolium (NBT) reduction test was carried out to measure ROS generation. The ratios of Mn-Cdots and ABTS were taken in the same dose to estimate the generation of ROS. The conversion of NBT (pale) to formazan (blue) was due to the production of ROS. The produced ROS was measured by the optical density of the obtained formazan at 575 nm. In Figure S12, increasing optical density for doses/concentration (D1, D2, and D3) confirms the ROS activity of the Mn-Cdots. The synergistic effect of Mn-Cdots and ABTS in the presence of white light led to the transfer of the electron to cellular oxygen, producing ROS that led to oxidative stress in the bacterial cell (Figure 6). A comparison table of the antibacterial activity of Mn-Cdots in the present study with the previously reported antibacterial activity of Cdots is given in Table S3. Notably, the antibacterial activity of Mn-Cdots is comparable with the previously reported Cdots-based antibacterial studies.[28−33]

The probable underlying mechanism for the antibacterial activity in the presence of photoexcited Mn-doped Cdots is the enhanced generation of ROS. It is well established that photoexcited Cdots can accept and donate electrons to the reaction medium.[34,35] Therefore, photoexcited Cdots can oxidize ABTS to the stable cation radical ($ABTS^{\bullet+}$) and serve as a shuttle for electrons that oxidize Mn(II) to Mn(III) present within Cdots.[36−38] The Mn(III) is able to oxidize Cdots (containing carboxyl groups) to anion radical ($CO^{2-\bullet}$), which might then reduce molecular oxygen to produce superoxide ($O^{2-\bullet}$), which is responsible for the generation of ROS.[38] Therefore, only Cdots (in the absence of Mn) do not show any significant antibacterial activity in the presence of light.

CONCLUSION

In summary, Mn-doped fluorescent Cdots were synthesized through a simple one-step hydrothermal method using guava leaves. These Mn-Cdots exhibited excellent antibacterial activity against Gram-negative bacteria *E. coli* in the presence of white light. The heightened antibacterial activity is attributed to the rapid generation of ROS because of the doping of a minute quantity of Mn in Mn-Cdots. A mediator ABTS was used along with Mn-Cdots that further contributed to the electron shuttler mechanism for the generation of ROS. Overall, the results provide the idea that Mn-Cdots in the presence of white lights might act as potent antibacterial agents, which shows outstanding possibilities to combat new antimicrobial resistance in the future.

ASSOCIATED CONTENT

Supporting Information

The Supporting Information is available free of charge at https://pubs.acs.org/doi/10.1021/acsomega.3c08586.

Experiments: Synthesis of Cdots, elemental analysis result of Mn Cdots (Table S1), elemental mapping analysis of Mn Cdots (Figure S1), EPR spectrum of Mn Cdots (Figure S2), PXRD spectra of Mn-Cdots (Figure S3), FTIR spectrum of Mn-Cdots (Figure S4), characterization of Cdots, including TEM images of Cdots (Figure S5), UV−visible spectrum of Cdots (Figure S6a), excitation-dependent on photoluminescence of Cdots (Figure S6b), EPR spectrum of Cdots (Figure S6c), FTIR of spectrum Cdots (Figure S6d), XPS spectrum of Cdots (Figure S7), elemental analysis result of Cdots (Table S2), elemental mapping analysis of Cdots (Figure S8), ionic strength-dependent study (Figure S9), pH-dependent study (Figure S10), photostability experiment (Figure S11), NBT test (Figure S12), and comparison table on antibacterial activity of

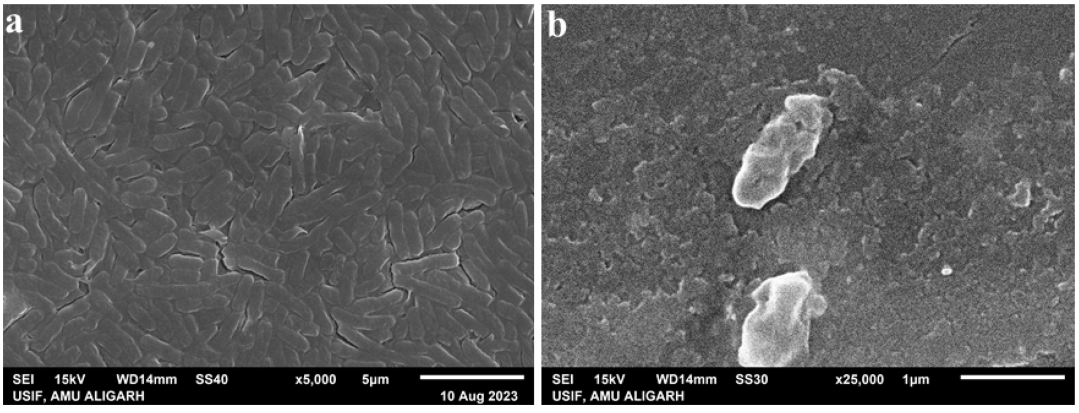

Figure 6. SEM images in different concentrations of *E. coli* bacteria that (a) present the untreated image of *E. coli* and (b) show the Mn-Cdots treated image of *E. coli* bacteria.

https://doi.org/10.1021/acsomega.3c08586
ACS Omega 2023, 8, 49460−49466

Mn Cdots of the present study with previously reported antibacterial activity of Cdots (Table S3) (PDF)

AUTHOR INFORMATION

Corresponding Authors

Md Palashuddin Sk − *Department of Chemistry, Aligarh Muslim University, Aligarh 202002 Uttar Pradesh, India;* orcid.org/0000-0003-2330-7382; Phone: (+91) 0571-2700920; Email: palashuddin.ch@amu.ac.in

Amaresh Kumar Sahoo − *Department of Applied Sciences, Indian Institute of Information Technology Allahabad, Prayagraj 211012 Uttar Pradesh, India;* orcid.org/0000-0002-9014-3317; Email: asahoo@iiita.ac.in

Authors

Mohammad Tariq − *Department of Chemistry, Aligarh Muslim University, Aligarh 202002 Uttar Pradesh, India*

Saurabh Shivalkar − *Department of Applied Sciences, Indian Institute of Information Technology Allahabad, Prayagraj 211012 Uttar Pradesh, India;* orcid.org/0000-0002-7912-1627

Hammad Hasan − *Department of Chemistry, Aligarh Muslim University, Aligarh 202002 Uttar Pradesh, India;* orcid.org/0000-0001-8344-5002

Complete contact information is available at: https://pubs.acs.org/10.1021/acsomega.3c08586

Author Contributions

M.T. performed all experiments, including the synthesis and characterization of Mn-Cdots, and wrote the original draft of the manuscript. S.S. conducted all the antibacterial experiments and helped to prepare the manuscript. H.H. helped and performed a few experiments. A.K.S. designed the antibacterial experiments, analyzed the data, and carried out the reviewing and editing of the manuscript. M.P.S. conceptualized and designed the experiments, analyzed the data, and wrote and reviewed the manuscript. The manuscript was written through the contributions of all authors. All authors have given approval to the final version of the manuscript.

Notes

The authors declare no competing financial interest.

ACKNOWLEDGMENTS

The authors thank the Department of Chemistry, University Sophisticated Instrument Facility (USIF), AMU, Aligarh & IIIT Allahabad for providing instrumental facilities and MNIT Jaipur for TEM and XPS facilities. Md Samim Hassan, Mostakim Sk, and Sangeeta Yadav are acknowledged for their help.

REFERENCES

(1) Zhou, Z.; Li, B.; Liu, X.; Li, Z.; Zhu, S.; Liang, Y.; Cui, Z.; Wu, S. Recent Progress in Photocatalytic Antibacterial. *ACS Appl. Bio Mater.* **2021**, *4* (5), 3909−3936.

(2) Alanis, J. A. Resistance to Antibiotics: Are We in the Post-Antibiotic Era? *Archives of Medical Research* **2005**, *36*, 697−705.

(3) O'Connell, M. G. K.; Hodgkinson, T. J.; Sore, F. H.; Welch, M.; Salmond, P. C.G.; Spring, R. D. Combating Multidrug-Resistant Bacteria: Current Strategies for the Discovery of Novel Antibacterials. *Angew. Chem., Int. Ed.* **2013**, *52*, 10706−10733.

(4) Chinemerem Nwobodo, D.; Ugwu, M. C.; Oliseloke Anie, C.; Al-Ouqaili, M. T. S.; Chinedu Ikem, J.; Victor Chigozie, U.; Saki, M. Antibiotic resistance: The challenges and some emerging strategies for tackling a global menace. *J. Clin Lab Anal.* **2022**, *36* (9), e24655.

(5) Zhu, H.; Peng, N.; Liang, X.; Yang, S.; Cai, S.; Chen, Z.; Yang, Y.; Wang, J.; Wang, Y. Synthesis, properties and mechanism of carbon dots-based nano-antibacterial materials. *Biomed. Mater.* **2023**, *18*, 062002.

(6) Đorđevic, L.; Arcudi, F.; Cacioppo, M.; Prato, M. A multifunctional chemical toolbox to engineer carbon dots for biomedical and energy applications. *Nat. Nanotechnol.* **2022**, *17*, 112−130.

(7) Anand, A.; Unnikrishnan, B.; Wei, S. C.; Chou, P. C.; Zhang, L. Z.; Huang, C. C. Graphene oxide and carbon dots as broad-spectrum antimicrobial agents-a minireview. *Nanoscale Horiz.* **2019**, *4*, 117−137.

(8) Li, P.; Sun, L.; Xue, S.; Qu, D.; An, L.; Wang, X.; Sun, Z. Recent advances of carbon dots as new antimicrobial agents. *SmartMater.* **2022**, *3*, 226−248.

(9) Li, X.; Fu, Y.; Zhao, S.; Xiao, J.; Lan, M.; Wang, B.; Zhang, K.; Song, X.; Zeng, L. Metal ions-doped carbon dots: Synthesis, properties, and applications. *Chem. Eng. J.* **2022**, *430*, 133101.

(10) Kailasa, S. K.; Koduru, J. R. Perspectives of magnetic nature carbon dots in analytical chemistry: From separation to detection and bioimaging. *Trends Environ. Anal. Chem.* **2022**, *33*, e00153.

(11) Desai, M. L.; Jha, S.; Basu, H.; Singhal, R. K.; Sharma, P. K.; Kailasa, S. K. Microwave-assisted synthesis of water-soluble Eu^{3+} hybrid carbon dots with enhanced fluorescence for the sensing of Hg 2+ ions and imaging of fungal cells. *New J. Chem.* **2018**, *42*, 6125−6133.

(12) Zoroddu, A. M.; Aaseth, A.; Crisponi, G.; Medici, S.; Peana, M.; Nurchi, M. V. The essential metals for humans: a brief overview. *J. Inorg. Biochem.* **2019**, *195*, 120−129.

(13) Sun, S.; Zhao, L.; Wu, D.; Zhang, H.; Lian, H.; Zhao, X.; Wu, A.; Zeng, L. Manganese-Doped Carbon Dots with Redshifted Orange Emission for Enhanced Fluorescence and Magnetic Resonance Imaging. *ACS Appl. Bio Mater.* **2021**, *4*, 1969−1975.

(14) Huang, X.; Wang, Z.; Li, S.; Lin, S.; Zhang, L.; Meng, Z.; Zhang, X.; Sun, S. Non-invasive diagnosis of acute kidney injury using Mn-doped carbon dots-based magnetic resonance imaging. *Biomater. Sci.* **2023**, *11*, 4289−4297.

(15) Han, C.; Xu, H.; Wang, R.; Wang, K.; Dai, Y.; Liu, Q.; Guo, M.; Li, J.; Xu, K. Synthesis of multifunctional manganese (ii)-carbon dots hybrid and its application as an efficient magnetic-fluorescent imaging probe for ovarian cancer cell imaging. *J. Mater. Chem. B* **2016**, *4*, 5798−5802.

(16) Irmania, N.; Dehvari, K.; Gedda, G.; Tseng, P. J.; Chang, J. Y. Manganese doped green tea derived carbon quantum dots as a targeted dual imaging and photodynamic therapy platform. *J. Biomed. Mater. Res. Part B Appl. Biomater.* **2020**, *108* (4), 1616−1625.

(17) Zhuo, S.; Fang, J.; Li, M.; Wang, J.; Zhu, C.; Du, J. Manganese (II)-doped carbon dots as effective oxidase mimics for sensitive colorimetric determination of ascorbic acid. *Microchim. Acta* **2019**, *186*, 745.

(18) Yang, X.; Hou, S.; Chu, T.; Han, J.; Li, R.; Guo, Y.; Gong, Y.; Li, H.; Wan, Z. Preparation of magnesium, nitrogen-codoped carbon quantum dots from lignin with bright green fluorescence and sensitive pH response. *Ind. Crops Prod.* **2021**, *167*, 113507.

(19) Yue, L.; Li, H.; Liu, Q.; Guo, D.; Chen, J.; Sun, Q.; Xu, Y.; Wu, F. Manganese-doped carbon quantum dots for fluorometric and magnetic resonance (dual mode) bioimaging and biosensing. *Microchim. Acta* **2019**, *186* (5), 315.

(20) Gutierrez-Montiel, D.; Guerrero-Barrera, L. A.; Chávez-Vela, A. N.; Avelar-Gonzalez, J. F.; Ornelas-García, G. I. Psidium guajava L.: From byproduct and use in traditional Mexican medicine to antimicrobial agent. *Front. Nutr.* **2023**, DOI: 10.3389/fnut.2023.1108306.

(21) Arshad, F.; Pal, A.; Rahman, A. M.; Ali, M.; Khan, A. J.; Sk, P. M. Insights on the solvatochromic effects in N-doped yellow-orange emissive carbon dots. *New J. Chem.* **2018**, *42*, 19837−19843.

(22) Bhati, A.; Anand, S. R.; Gunture; Garg, A. K.; Khare, P.; Sonkar, S. K. Sunlight-Induced Photocatalytic Degradation of Pollutant Dye by Highly Fluorescent Red-Emitting Mg-N-Embedded Carbon Dots. *ACS Sustainable Chem. Eng.* **2018**, *6* (7), 9246−9256.
(23) Doren, A.; Genet, J. M.; Rouxhet, G. P. Analysis of Poly(Ethylene Terephthalate)(PET) by XPS. *Surf. Sci. Spectra* **1994**, *3* (4), 337−341.
(24) Peana, M.; Medici, S.; Nurchi, M. V.; Crisponi, G.; Lachowicz, I. J.; Zoroddu, A. M. Manganese and cobalt binding in a multi-histidinic fragment. *Dalton Trans.* **2013**, *42*, 16293−16301.
(25) Bennur, T. H.; Srinivas, D.; Ratnasamy, P. EPR spectroscopy of copper and manganese complexes encapsulated in zeolites. *Microporous Mesoporous Mater.* **2001**, *48*, 111−118.
(26) Xu, D.; Jiao, R.; Sun, Y.; Sun, D.; Zhang, X.; Zeng, S.; Di, Y. L-Cysteine-Assisted Synthesis of Urchin-Like γ-MnS and Its Lithium Storage Properties. *Nanoscale Res. Lett.* **2016**, *11*, 444.
(27) Kumar, S.; Nath, P. Absorption spectra of Mn2+ ion in glasses. *Trans. Indian Ceram. Soc.* **1966**, *25*, 12−19.
(28) Tariq, M.; Singh, A.; Varshney, N.; Samanta, K. S.; Sk, P. M. Biomass-derived carbon dots as an emergent antibacterial agent. *Materials Today Communications* **2022**, *33* (33), 104347.
(29) Saravanan, A.; Maruthapandi, M.; Das, P.; Luong, T. H. J.; Gedanken, A. Green Synthesis of Multifunctional Carbon Dots with Antibacterial Activities. *Nanomaterials* **2021**, *11* (2), 369.
(30) Wang, H.; Zhang, M.; Ma, Y.; Wang, B.; Shao, M.; Huang, H.; Liu, Y.; Kang, Z. Selective inactivation of Gram-negative bacteria by carbon dots derived from natural biomass: *Artemisia argyi* leaves. *J. Mater. Chem. B* **2020**, *8*, 2666−2672.
(31) Verma, A.; Arshad, F.; Ahmad, K.; Goswami, U.; Samanta, K. S.; Sahoo, K. A.; Sk, P. M. Role of surface charge in enhancing the antibacterial activity of fluorescent carbon dots. *Nanotechnology* **2020**, *31*, 095101.
(32) Saravanan, A.; Maruthapandi, M.; Das, P.; Ganguly, S.; Margel, S.; Luong, T. H. J.; Gedanken, A. Applications of N-Doped Carbon Dots as Antimicrobial Agents, Antibiotic Carriers, and Selective Fluorescent Probes for Nitro Explosives. *ACS Appl. Bio Mater.* **2020**, *3* (11), 8023−8031.
(33) Sun, B.; Wu, F.; Zhang, Q.; Chu, X.; Wang, Z.; Huang, X.; Li, J.; Yao, C.; Zhou, N.; Shen, J. Insight into the effect of particle size distribution differences on the antibacterial activity of carbon dots. *J. Colloid Interface Sci.* **2021**, *584*, 505−519.
(34) Wang, X.; Cao, L.; Lu, F.; Meziani, M. J.; Li, H.; Qi, G.; Zhou, B.; Harruff, B. A.; Kermarrec, F.; Sun, Y.-P. Photoinduced electron transfers with carbon dots. *Chem. Commun.* **2009**, 3774−3776.
(35) Srivastava, N.; Khamo, S. J.; Pandit, S.; Fathi, P.; Huang, X.; Cao, A.; Haasch, T. R.; Nie, S.; Zhang, K.; Pan, D. Influence of Electron Acceptor and Electron Donor on the Photophysical Properties of Carbon Dots: A Comparative Investigation at the Bulk-State and Single-Particle Level. *Adv. Funct. Mater.* **2019**, *29*, 1902466.
(36) Song, Y.; Jiang, J.; Ma, J.; Pang, S.-Y.; Liu, Y.-z.; Yang, Y.; Luo, C.-w.; Zhang, J.-q.; Gu, J.; Qin, W. ABTS as an Electron Shuttle to Enhance the Oxidation Kinetics of Substituted Phenols by Aqueous Permanganate. *Environ. Sci. Technol.* **2015**, *49* (19), 11764−11771.
(37) Huang, Y.; Lin, J.; Zou, J.; Xu, J.; Wang, M.; Cai, H.; Yuan, B.; Ma, J. ABTS as an electron shuttle to accelerate the degradation of diclofenac with horseradish peroxidase-catalyzed hydrogen peroxide oxidation. *Science of The Total Environment* **2021**, *798*, 149276.
(38) Collins, J. P.; Dobson, W. D. A.; Field, A. J. Reduction of the 2,29-Azinobis(3-Ethylbenzthiazoline-6-Sulfonate) Cation Radical by Physiological Organic Acids in the Absence and Presence of Manganese. *Appl. Environ. Microbiol.* **1998**, *64*, 2026−2031.

https://doi.org/10.1021/acsomega.3c08586
ACS Omega 2023, 8, 49460−49466